Preprints of the 21st IFAC World Congress (Virtual)
Berlin, Germany, July 12-17, 2020

An Artificial Potential Function For Battery Life Optimization In Car-following System ⋆

Bo Liu * **Yingze Yang** ** **Hongtao Liao** * **Rui Zhang** *
Bin Chen * **Kai Gao** *** **Feng Zhou** **** **Weirong Liu** **
Zhiwu Huang * **Jun Peng** **

* *School of Automation, Central South University, Changsha, China, 410083 (corresponding author e-mail: kai-g@csust.edu.cn)*
** *School of Computer Science and Engineering, Central South University, Changsha, China, 410083*
*** *College of Automotive and Mechanical Engineering, Changsha University of Science & Technology, Changsha, China, 410114*
**** *School of Electrical & Information Engineering, Changsha University of Science & Technology, Changsha, China, 410114*

Abstract: For a pure electric car-following system, if the auto-following vehicle acts in an aggressive following manner, battery life fades evidently, since overcharging or over-discharging damage the cell irreversibly. In this regard, this paper proposed an artificial potential function for battery life extension. First, the electric vehicle physical model and an empirical lithium-ion battery model have established form real-world data measurement. The physical layer models car-following dynamics and the battery model describes the energy consumption. Second, with the perceptive of the battery life in a loss-minimal, optimize manner, the controller mathematically computes the optimal acceleration/deceleration value with the Lagrange multipliers method. Then using the Matlab curve fitting tool toolbox to fusion optimal acceleration data with potential function, thus the acceleration consistent rule is realized through the consistency of an artificial potential function. Finally, the control strategy is validated through a simulation test in Matlab/Simulink, and the results show that the proposed control strategy extends battery life while keeping good tracking ability.

Keywords: car-following control strategy, battery life optimization, artificial potential function.

1. INTRODUCTION

Recent studies have been started to explore the introduction of multi-objective, e.g. spacing control, electricity economy, and string ability analysis, into the car-following system Li et al. (2010). The game theory techniques consider each autonomous vehicle as an agent, and the controller design is seen as a game between the actions of each agent and the disturbances introduced by the environment Li et al. (2017a). But, this approach has exponential complexity. In Luo et al. (2015), the author proposed a position-based nonlinear model predictive control strategy for the i-Hybrid electric vehicle, which coordinates tracking safety, fuel consumption, and ride comfort subject to terminal constraints on stable tracking. Although model predictive control is a promising way to solve the multi-objective problem, it shows undesired computational complexity. Thus, game theory and model predictive control both cannot easily embed multiple design objectives in battery life optimal applications.

It is noted that for a pure electric car-following system, the performance is highly dependent on energy storage devices functionality to predict and control critical health issues Asadi and Vahidi (2010). And in the car-following scenario, the rear car needs frequent acceleration and deceleration to ensure the desired distance, and this has a great impact on battery life. Thus, accurate and instantaneous information on the state of the battery, such as state of charge and state of health, should be considered into a car-following control strategy to guarantee safe and reliable battery operation He et al. (2012). But, most work only focuses on the lifetime of batteries due to degradation that occurs with cycling and calendar aging.

To this point, a feasible and effective algorithm with low computational complexity is needed. In this paper, we first model the car-following system dynamics. Then find the coefficient of each vector in the linear combination of the gradients of the constraint equation by solving the system of equations. Lastly, using the Matlab cftool to fusion optimal acceleration data with potential function, so the acceleration consistent rule is realized through the consistency of an artificial potential function. Thus, artificial potential functions based on the Lagrange multipliers method are developed as a control strategy, with percep-

⋆ This work partially supported by National Nature Science Foundation of China (Grant Nos. 61672537, 61672539). Corresponding author: Kai Gao,E-mail address: kai-g@csust.edu.cn

tive of the battery state of charge and state of health in a loss-minimal, optimized manner.

The paper organized as follows: electric vehicle longitudinal dynamic model are constructed in Sec. 2. In Sec. 3, the Lagrange multiplier method based Artificial Potential Function control strategy is designed. Then experiments are conducted to prove the effectiveness of the control strategy followed with result analysis and conclusion summarized in Sec. 4 and Sec. 5, respectively.

2. ELECTRIC VEHICLE LONGITUDINAL DYNAMIC MODEL

As sketched in Fig. 1, the green area represent a relative safe position and domain by attractive force, while the distance between $d_{safe,\max}$ and $d_{safe,\min}$ denote the warning distance, which affected by repulsive force. And the $d_{safe,\min}$ are the minimum distance when drive into this area, enormous repulsive force will be added.

2.1 Electric vehicle powertrain model

In this paper, we use the energy consumption model in Li et al. (2017b), which is a quasi-steady backward approach.

$$P_t = (\alpha {v_f}^2 + f_r mg + \frac{bv_f}{R_t}) \cdot v_f \tag{1}$$

where $\alpha = 0.5\rho C_D A_f$ is the aerodynamic resistance constant determined by air density ρ, A_f is the frontal area of the EV ($1.8\ m^2$), C_D is the coefficient of drag (0.3); f_r is the rolling resistance constant (0.015); g is the gravity acceleration; v_f is the velocity of vehicle; b is the bearings damping coefficient ($1.0\ m$) and R_t is an vehicle tire radius ($0.3\ m$).

The motor power loss expression and regenerative braking power is defined as below:

$$P_m = \frac{r \cdot R_t}{K^2} \cdot (ma_f + \alpha {v_f}^2 + f_r mg + \frac{bv_f}{R_t})^2 \tag{2}$$

$$P_g = \eta_g m a_f v_f \tag{3}$$

where r is the resistance of the conductor, η is the efficiency of the generator. The DC-DC converter loss $\eta_{DC} = 0.96$ for battery and ancillary power $P_a = 7.0Kw$ is consider as the constant, which not determined by velocity and acceleration. This part can described as:

$$P_{loss} = (1 - \eta_{DC}) P_{bat} + P_a \tag{4}$$

Based on the above introduce, the instantaneous power of a pure electric vehicle can be measured with the equation below:

$$P_{bat} = P_t + P_m + P_g - P_{loss} \tag{5}$$

As treated in paper Li et al. (2017b), these source of power consumption are assumed to be mostly independent, and thus their effects can be summed up to embody the total energy consumption.

2.2 Lithium battery model

(a) SOC-OCV model The internal resistance model as follows:

$$V_{cell}(k) = U(k) - i(k) \cdot R \tag{6}$$

where V_{cell}, U, i and R represents the terminal voltage,open-circuit voltage, current, and internal resistance of cell at time sequence k, respectively.

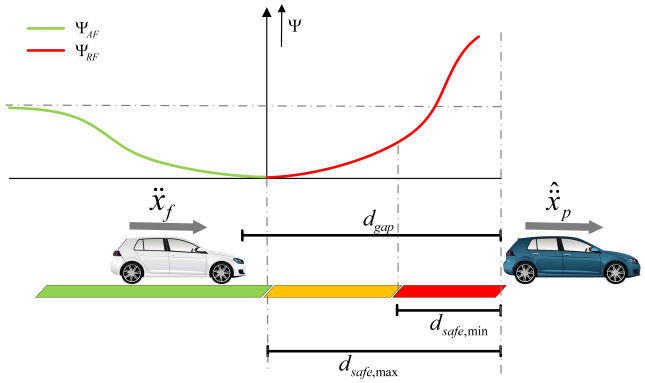

Fig. 1. Side view of car-following system

A function describes the quantitative relationship between state-of-charge Open Circuit Voltage (OCV) Rahimi-Eichi et al. (2013) is used to calculate $V_{ocv}(k)$, which is defined as:

$$\begin{cases} V_{ocv}(w) = K_0 - \frac{K_1}{w} - K_2 w + K_3 \ln(w) + K_4 \ln(1-w) \\ V_{cell}(k) = V_{ocv} - R \cdot i \end{cases} \tag{7}$$

where w, V_{ocv}, $V_{cell}(k)$ is the battery SOC, instantaneous OCV, measured cell voltage, respectively. Thus, the parameters K_0, K_1, K_2, K_3, K_4 can map the current SOC estimation value onto an accurate OCV.

Given the terminal cell power $P_{bat} = V_{ocv} \cdot I_{bat}$, And then the SOC dynamics can be delineated by

$$soc(k+1) = soc(k) - \frac{i(k) \cdot \Delta t}{Q} \tag{8}$$

where soc, Q, and Δt are the cell SOC, the nominal cell capacity, and the sampling interval, respectively. The following electrical constrains must be fufilled when operating the EV powertrain:

$$i_{\min} \le i(k) \le i_{\max}$$

$$soc_{\min} \le soc(k) \le soc_{\max}$$

where $i_{\min}$ and $i_{\max}$ are the cell current bounds (maximum charge/discharge current); $soc_{\min}$ and $soc_{\max}$ are the SOC bounds.

(b) Health model A semi-empirical life model is adopted in this paper to simulate the capacity loss of the battery cell. The activation energy E_a in$[J/mol]$ and the power-law factor z are determined by:

$$E_a(c) = 31700 - 370.3c \quad z = 0.55$$

It note that 20% capacity loss is considered as end-of-life(EOL) of automotive battery, and the total discharge Ah throughput A_{tol} is, therefore, acquired by:

$$A_{tol}(c, T_c) = \left[\frac{20}{M(c) \cdot \exp(\frac{E_a(c)}{R_c T_c})} \right]^{1/z} \tag{9}$$

where $M(c)$ is a function of the C-rate, T_c, R_c is the lumped battery temperature in $313K(40^oC)$, ideal gas constant $8.31J/mol \cdot K$. As a result, the dynamic state-of-health (SOH) model is thereby established as Ebbesen et al. (2012)

$$soh(k+1) = soh(k) - \frac{|i(k)| \cdot \Delta t}{7200 A_{tol}(c, T_c)} \tag{10}$$

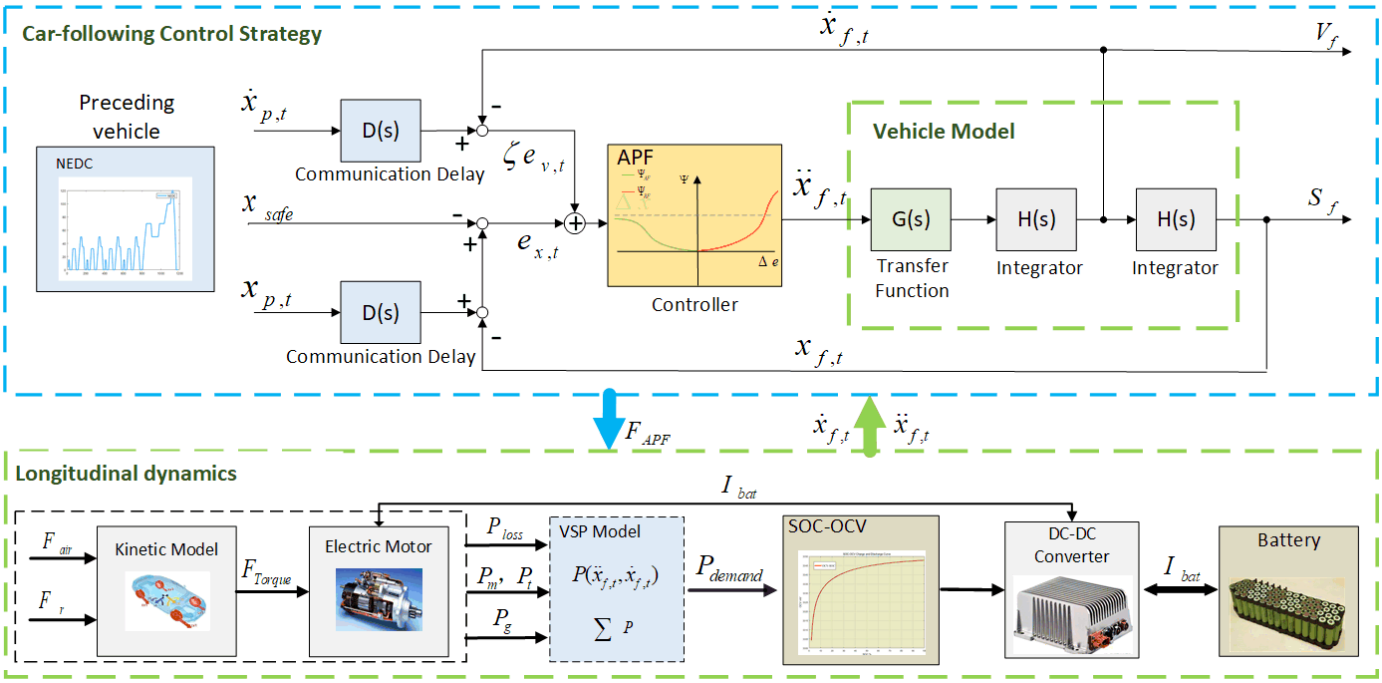

Fig. 2. Car-following control strategy and global longitudinal dynamics of pure electric vehicle

based on the SOH model, the values of SOH can be calculated.The following health constraints must be fulfilled when calculated the powertrain:

$$soh_{\min} \leq soh(k) \leq soh_{\max}$$

where $soh_{\min}$ and $soh_{\max}$ are the SOH bounds.

3. CAR-FOLLOWING CONTROL STRATEGY

In this section, we modeling the car-following system, and use Lagrange multipliers method (LMM) to design an artificial potential function controller by take battery health into consideration.

3.1 Car-following system model

The inter-distance dynamics can be represented as a double integrator driven by the difference between the leader vehicle acceleration $\ddot{x}_p$ and the follower vehicle acceleration $\ddot{x}_f$ as depicted below:

$$\ddot{d}_{gap} = \ddot{x}_p - \ddot{x}_f, \tag{11}$$

where $\ddot{d}_{gap}$ is the gap between the two vehicles, and the safety constrains are shown in Fig. 1. By setting corresponded maximum braking capacity and maximum speed, the safe inter-distance that avoids collision is obtained

$$\lambda = \frac{27{B^2}_{\max}}{8(\dot{e}_v(0) + \dot{e}_x(0))^3},$$

$${V^r}_{\max} = e_{v,max} + \frac{\lambda}{2} e_{x,\max},$$

$$d_{safe,\max} = \frac{0.77({V^r}_{\max})^2}{B_{\max}} + d_{safe,\min},$$

where $B_{\max}$, ${V^r}_{\max}$ are set according to the real driving situation, and we assume an deceleration potential of $B_{\max} - 3m \cdot s^{-2}$, reference velocity ${V^r}_{\max} = 120km \cdot h^{-1}$ for a given road and constant weather condition.

3.2 Artificial potential function design

The artificial potential field provides a more flexible way to deal with real-time constraints Wu et al. (2020). At the decelerating and accelerating stage, the initial speed is divided into l ($l = v_0/\Delta$), equal portions with interval Δ that refer to the time of wireless communication delay, which is assumed that acceleration remains constant during each interval Δ. The time spent in changing speed during the ith interval t_i is the ratio of the deviation of speed Δ divided by the constant acceleration a_i during the ith interval. Besides, the distance x_i driven during each interval is given by:

$$x_i = \frac{(v_0 + i\Delta)^2 - [v_0 + (i-1)\Delta]^2}{2a_i} \tag{12}$$

The constraint in the car-following regime is :

$$\sum_{j=1}^{i} x_j = x_{safe} + v_f \sum_{j=1}^{i} t_i - x_{gap} \tag{13}$$

where $\sum_{j=1}^{i} x_j$ is the distance passed by the subjects vehicle, x_{safe} is the initial headway spacing between two vehicles, x_{gap} is the final headway spacing between two vehicles when they reach the same level of speed, $\sum_{j=1}^{i} t_i$ is the time spent. In dynamic driving situations, the leading vehicle may change speed frequently. Therefore, during each time interval from wireless communication, the controller receives changes in leading vehicles speed computer the optimal acceleration/deceleration value with Lagrange multipliers method accordingly.

The control scheme is shown in Fig. 2, where $x_{p,f}$, $\dot{x}_{p,f}$, is the position of preceding car i.e. the leader vehicle, $e_{x,t}$, $e_{v,t}$ is the tracking error of the position, velocity respectively. $D(s) = e^{-\tau s}$, τ denote the latency induced by the wireless

communication. $H(s) = 1/s$ represents the integrator in simulation.

From Milanés and Shladover (2014), a generalized vehicle longitudinal dynamic is described by a first-order transfer function:

$$G(s) = \frac{1}{Ts+1} \tag{14}$$

where T is a time-constant representing drive-line dynamics. To obtain the closed-loop and design $\ddot{x}_f$, it is required to have a balanced use of the position error and the velocity error in a single controller design, thus we adopted the coordinate transformation in Milanés et al. (2013). The error state $\mathbf{e_f}$ can be defined as:

$$\mathbf{e_f} = \begin{pmatrix} e_{x,t} + \zeta e_{v,t} \\ e_{v,t} \\ \dot{e}_{v,t} \end{pmatrix} \tag{15}$$

where the constant ζ determines the weight of $e_{v,t}$ with respect to $e_{x,t}$, i.e. it determines the ratio for system damping. The dynamics can be described by:

$$\begin{pmatrix} x_t \\ \dot{x}_t \\ \ddot{x}_t \end{pmatrix} = \mathbf{e_f} + \frac{1}{T}\left(u_{t-1} - \bar{u}_t\right) \tag{16}$$

and the control input $\bar{u}_t$ is then designed through potential function with Lagrange multipliers.

The upper control loop strategy have a direct influence on inner loop, i.e. battery system. More specifically, based on the Eq(2),(7),(10), the two coupled loops can be linked by the following approximate relationship:

$$soh \propto \dot{i}_{bat} \propto \dot{a}_f \tag{17}$$

which means that the battery life has a direct relationship with the current change rate, also, proportional to acceleration change rate. Therefore, the cumulative SOH loss ϑ during a time period t (unit in s) is expressed as:

$$\vartheta(a,t) = \int_0^t \frac{|a|}{7200 A_{tol}(c, T_c)} dt \tag{18}$$

The primary objective is to minimize the cumulative SOH loss $\vartheta(a,t)$ to extend the battery life. The optimal a^* could be obtained as a result of Eq(19)

$$\frac{\partial \vartheta}{\partial a} = 0 \tag{19}$$

To minimize $\vartheta(a,t)$, a technique for solving optimization problems with multiple constraints Bertsekas (2014) is designed. As one constraint regarding the headway spacing between the leader and the follower, thus one Lagrange multiplier κ is added to formulate a Lagrange function based on the objective function Eq(18). In this case, Lagrange multiplier κ means the rate at which the optimal cumulative SOH loss value changes if such constraint changes, resulting in optimal acceleration a^* during each interval Δ and one optimal Lagrange multiplier κ^*:

$$Z(x) = \sum_{j=1}^{i} x_j - x_{safe} - v_f \sum_{j=1}^{i} t_i + x_{gap} = 0 \tag{20}$$

$$H(x,\kappa) = \vartheta(a,t) + \kappa Z(x) \tag{21}$$

$$\frac{\partial H(x,\kappa)}{\partial a} = 0, \frac{\partial H(x,\kappa)}{\partial \kappa} = 0 \tag{22}$$

It is noted that this method is easy to integrate, due the result can be fitted into a polynomial form by Matlab cftool, i.e. linear function. In this case, we can use this linear function of acceleration a^* during each interval Δ to design an artificial potential function in deceleration and acceleration process, while guarantee the battery life. Thus, a Lagrange multipliers method based artificial potential function (LMM-APF), which consider the battery life influences and characteristics between acceleration and deceleration process, is presented:

$$\begin{cases} \psi_{RP}(x_t) = c_1 {x_t}^4 - c_2 {x_t}^3 + c_3 {x_t}^2, d_{gap} \geq d_{safe,\min} \\ \psi_{RP}(x_t) = c_4(1 - \exp(-c_5(x_t - c_0)))^2, d_{gap} \leq d_{safe,\min} \\ \psi_{AP}(x_t) = c_6(1 - \exp(-c_7 x_t))^2, d_{gap} \leq d_{safe,\max} \end{cases} \tag{23}$$

where $\mathbf{c} = [\, c_1\ c_2\ c_3\ c_4\ c_5\ c_6\ c_7 \,]$ are the design parameters. It note that the equilibrium state of the desired inter-vehicle distance, i.e. c_0, can be obtained by setting the derivative of such a potential function to control the potential towards zero. The artificial potential function parameters are determined when knowing the optimal results from solving the Eq(20),(21),(22). In this paper, the optimize parameter results are $\mathbf{c} = [\, 0.05\ 0.06\ 0.4\ 184.05\ 0.15\ 178.03\ 0.1 \,]$. From its definition, a global minimum of this function is at the point of d_{safe}, if the condition $c_1 \cdot c_2 \cdot c_3 \cdot c_4 \cdot c_5 \cdot c_6 \cdot c_7 > 0$ are satisfied.

Based on Eq(16),(15), use the derivative of such a function to control the potential towards zero, thus the control input $\bar{u}_t$ is defined below:

$$\bar{u}_t = \frac{\partial \psi(\mathbf{e_{f,11}})}{\mathbf{e_{f,11}}} + u_{t-1} \tag{24}$$

where $\partial\psi(\mathbf{e_{f,11}})$ is chosen in Eq(23). Then, the battery health and gap-closing state can be restricted within the normal operational range. Furthermore, models defined here can be used to fill the gap between experimental results on a car simulation software and a microscopic simulation.

4. EXPERIMENTS AND RESULTS

This section evaluated the car-following system performance with the tracking capability and energy perspective. To perform the simulations, the specifications of the principle powertrain components parameters and the battery are listed as follow: (a) battery internal resistance is 0.01 Ohm; battery Nominal capacity is 2.3 Ah; maximal charge current -35 A; maximal discharge current 70 A; initial SOC is 100%; initial SOH is 100%; (b) $a_{\max}$ is 3 $m \cdot s^{-2}$; $a_{\min}$ is -3 $m \cdot s^{-2}$;

The presented approach is evaluated with the real driving cycle from NEDC. In the paper, to determine the tracking capability, index S is defined in terms of the error in the speed and the error in the distance as:

$$S = \frac{1}{n} \sum_{i=1}^{p} \left(\left| \frac{\Delta v(i)}{K_{DV}} \right| + |\Delta d(i)| \right) \tag{25}$$

Where K_{DV} is a weighting coefficient, and n is the length of Δd to calculate S.

Due to space limitations, only the comparing results of the NEDC driving cycle with the period of the first 600s are shown in Fig 3 and Fig 4, with an intuitive view of speed track in the first 13s driving cycle. In Fig 3, the good behavior of the tracking capability can be appreciated,

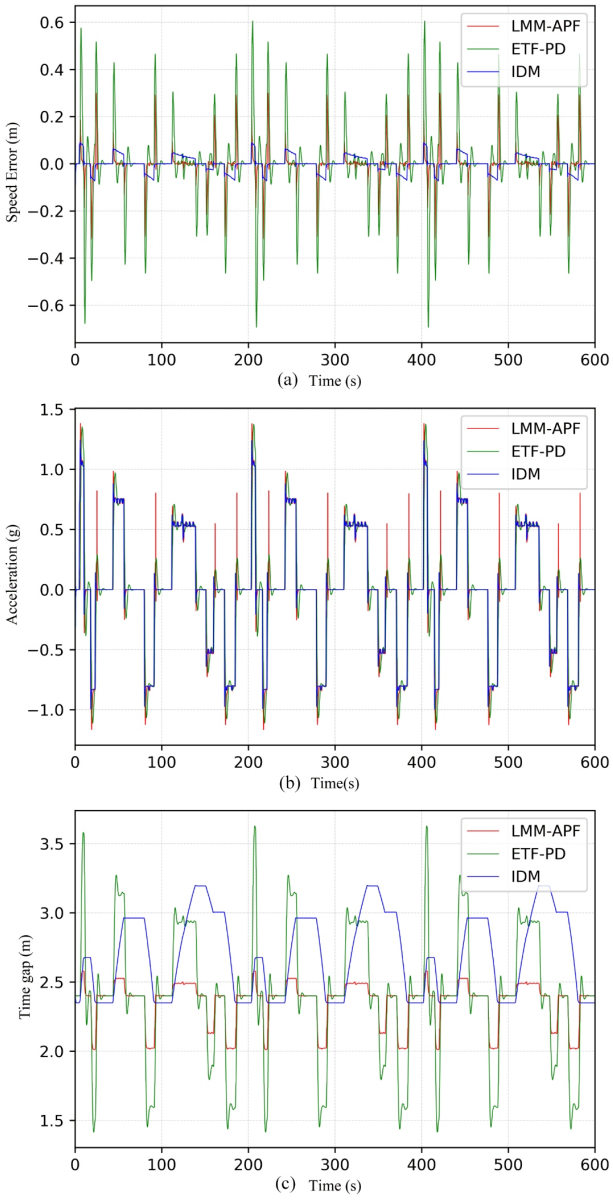

Fig. 3. Tracking capability comparison among LMM-APF, ETF-PD and IDM control strategy, (a) is the speed error from the leader; (b) is the acceleration distribution ; (c) is time gap keeping, initial at 2.4 m

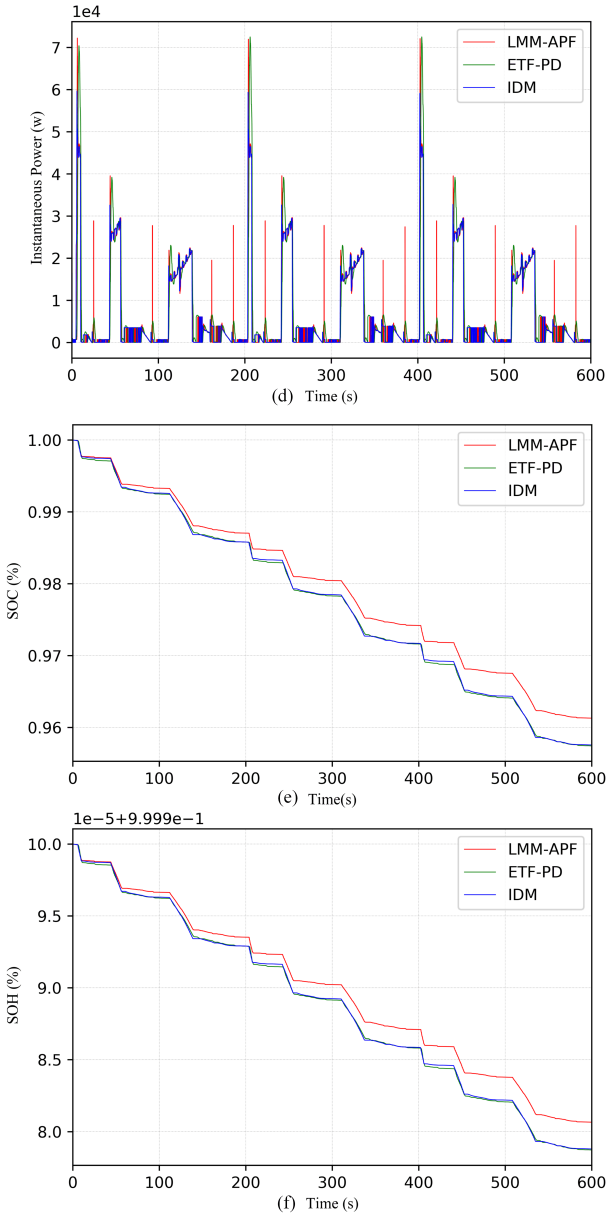

Fig. 4. Battery state comparison among LMM-APF, ETF-PD and IDM control strategy, (d) is instantaneous power output; (e) is SOC sustenance in %; (f) is SOH sustenance in %

due to the simplicity of transfer function. The results indicate that: (1) as depicted in picture (c), the ETF-PD controller implemented in our control scheme does not perceptibly follow the position changes of the preceding vehicle, leaving behind with big time gap. (2) as depicted in picture (a), the IDM controller are quite sensitive to the change of speed, following tightly to the speed variations of leader. It can represent the scenario that drivers operate their vehicles more aggressively on a road without hesitation; (3) LMM-APF controller overcome these drawbacks, providing smooth and stable car following responses.

The differences appearing on Fig 4 indicate that the acceleration control strategy may be considered as a major factor of influence on the battery life, and this point will be illustrated. Although the speed tracking is pretty similar for all the vehicles see Fig 5, it is noted that IDM act most frequently, while ETF-PD suffers from response lag effect and caused big overshot. Thus the battery current curve would be more smooth and preferred.

Detailed tracking capability, acceleration rate, and tracking capability are summarized in Tab 1. The acceleration rate standard deviation revealed that LMM-APF controller caused the least fluctuation with numerical result in 0.49, followed by IDM with numerical result in 0.74, while ETF-PD in 1.52. The tracking capability is a sign of car-following system's performance. In this regard, all of the systems exhibited relatively good tracking safety with a tracking capability index below 0.7. LMM-APF tracking

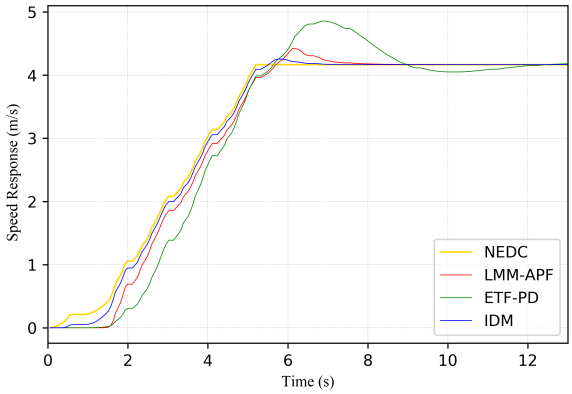

Fig. 5. NEDC speed track comparison among LMM-APF, ETF-PD and IDM

Table 1. Acceleration rate and tracking capability experimental results

Model	Acceleration rate	Tracking capability
IDM	0.74	0.32
LMM-APF	0.49	0.65
ETF-PD	1.52	0.63

Table 2. Battery state and energy consumption experimental results

Model	SOH	SOC	Power consumption (J)
IDM	-9.5%	-0.8%	3.4×10^6
LMM-APF	3.5%	-1.2%	3.46×10^6
ETF-PD	-6%	-0.77%	3.8×10^6

capability index was 0.65, which was essentially equal to the ETF-PD value of 0.63 and was exceeded by the IDM tracking capability index of 0.32.

Table 2 summarizes the experimental results for the SOH and SOC deviation from the preceding vehicle and tracking capability during the driving cycle. It can be found that the proposed LMM-APF control strategy works well to ensure the battery charge and discharge sustenance, while extend battery life to 3.5%, with a loss SOC value at -1.2%. It is noted that, in energy view, although IDM consumes the least energy due to is good tracking capability, LMM-APF power consumption value was 3.46×10^6, which was essentially equal to the IDM value of 3.4×10^6 and was exceeded by the ETF-PD power consumption value of 3.46×10^6.

5. CONCLUSION

In this paper, artificial potential function with Lagrange multipliers was proposed for car-following system optimization of battery life. It was found that without sacrificing safety, and keeping a relatively good tracking performance, the proposed control strategy can extend the SOH value by 3.5% with SOC loss in value of 1.2% under 600s NEDC driving cycle, due to smooth transition between acceleration and deceleration. Although, the IDM model producing smooth car-following behavior, the SOH value declined by 9.5%, due to its aggressive way of following manners. Meanwhile, the ETF-PD model consumed the most power in the whole process, due to slow response and large clearance gap variations.

ACKNOWLEDGEMENTS

This work is partially supported by National Natural Science Foundation of China (Grant Nos. 61672537, 61672539)

REFERENCES

Asadi, B. and Vahidi, A. (2010). Predictive cruise control: Utilizing upcoming traffic signal information for improving fuel economy and reducing trip time. *IEEE transactions on control systems technology*, 19(3), 707–714.

Bertsekas, D.P. (2014). *Constrained optimization and Lagrange multiplier methods*. Academic press.

Ebbesen, S., Elbert, P., and Guzzella, L. (2012). Battery state-of-health perceptive energy management for hybrid electric vehicles. *IEEE Transactions on Vehicular technology*, 61(7), 2893–2900.

He, H., Xiong, R., and Guo, H. (2012). Online estimation of model parameters and state-of-charge of lifepo4 batteries in electric vehicles. *Applied Energy*, 89(1), 413–420.

Li, N., Oyler, D.W., Zhang, M., Yildiz, Y., Kolmanovsky, I., and Girard, A.R. (2017a). Game theoretic modeling of driver and vehicle interactions for verification and validation of autonomous vehicle control systems. *IEEE Transactions on control systems technology*, 26(5), 1782–1797.

Li, S., Li, K., Rajamani, R., and Wang, J. (2010). Model predictive multi-objective vehicular adaptive cruise control. *IEEE Transactions on Control Systems Technology*, 19(3), 556–566.

Li, Y., Zhang, L., Zheng, H., He, X., Peeta, S., Zheng, T., and Li, Y. (2017b). Nonlane-discipline-based car-following model for electric vehicles in transportation-cyber-physical systems. *IEEE Transactions on Intelligent Transportation Systems*, 19(1), 38–47.

Luo, Y., Chen, T., Zhang, S., and Li, K. (2015). Intelligent hybrid electric vehicle acc with coordinated control of tracking ability, fuel economy, and ride comfort. *IEEE Transactions on Intelligent Transportation Systems*, 16(4), 2303–2308.

Milanés, V. and Shladover, S.E. (2014). Modeling cooperative and autonomous adaptive cruise control dynamic responses using experimental data. *Transportation Research Part C: Emerging Technologies*, 48, 285–300.

Milanés, V., Shladover, S.E., Spring, J., Nowakowski, C., Kawazoe, H., and Nakamura, M. (2013). Cooperative adaptive cruise control in real traffic situations. *IEEE Transactions on Intelligent Transportation Systems*, 15(1), 296–305.

Rahimi-Eichi, H., Baronti, F., and Chow, M.Y. (2013). Online adaptive parameter identification and state-of-charge coestimation for lithium-polymer battery cells. *IEEE Transactions on Industrial Electronics*, 61(4), 2053–2061.

Wu, Y., Huang, Z., Liao, H., Chen, B., Zhang, X., Zhou, Y., Liu, Y., Li, H., and Peng, J. (2020). Adaptive power allocation using artificial potential field with compensator for hybrid energy storage systems in electric vehicles. *Applied Energy*, 257, 113983.